

A magnetically coupled 2-D waveguide power transfer

Yuichi Masuda
 Graduate school of Frontier Science
 The University of Tokyo
 Chiba, Japan
 masuda@hapis.k.u-tokyo.ac.jp

Hiroyuki Shinoda
 Graduate school of Frontier Science
 The University of Tokyo
 Chiba, Japan
 hiroyuki_shinoda@k.u-tokyo.ac.jp

Abstract— We propose a coil-patterned waveguide sheet for magnetic coupling in a 2-D waveguide power transfer system (2DWPT). In magnetic resonance wireless power transfer, the coupling coefficient decreases due to flux leakage. Our proposed system can extend the length of the Tx waveguide sheet without reducing the coupling coefficient. The leakage flux can be adjusted by reducing the group velocity in the waveguide sheet. The effectiveness of this waveguide power transfer method is supported by simple theoretical analyses. Our simulation and measurement results concur with the analytical findings and demonstrate that the proposed waveguide sheet can be extended while maintaining practical efficiency.

Keywords—magnetic resonance, 2-D waveguide power transfer, wireless power transfer, SAR.

I. INTRODUCTION

Efficiency drops due to leakage flux are a common problem in magnetic coupling for wireless power transfer (WPT)[1][2]. There is a trade-off between the positional misalignment between coils and leakage flux; as one increases, the other also tends to increase [3][4]. WPT systems with multiple Tx coils represent one of the promising forms of dynamic WPT applications [5]-[8]. By switching the Tx coil as the Rx coil moves, the range of WPT can be extended while maintaining efficiency. The size of each Tx coil is adjusted to take leakage flux into account.

A 2-D waveguide power transfer (2DWPT) system [9][10] offers another solution for dynamic WPT. In a 2DWPT system, an electromagnetic (EM) wave that propagates in the waveguide sheet can be wirelessly extracted by the Rx coupler, which is placed on the sheet with a small gap. Since most of the EM energy is confined within the simple waveguide sheet, the range of 2DWPT can be expanded at a low cost by lengthening the sheet.

In this paper, we propose a magnetically coupled 2DWPT system with a coil-patterned waveguide sheet. The wavelength in the sheet is adjusted by considering both leakage flux and propagation loss. The group velocity in the sheet is extremely slow compared to that in a vacuum. The extracted efficiency does not decrease when the length of the sheet is extended, as the supplied energy is not instantaneously diffused throughout the sheet. "Extracted efficiency" refers to the ratio of EM energy extracted by the Rx coil from the sheet.

The rest of this paper is organized as follows: Section II presents the equivalent circuit and a simple theoretical analysis, clarifying the trade-off between extracted efficiency and

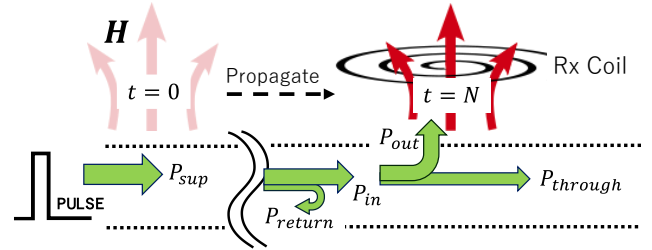


Fig. 1. Behavior of EM waves when pulsed waves are input. A uniform magnetic field is not formed over the entire sheet. Therefore, the leakage flux can be minimized.

propagation loss. Section III describes the proposed coil-patterned waveguide sheet. Full-wave simulation results show the relationship between the sheet length and extracted efficiency. The specific absorption rate (SAR) [11] is also evaluated. Section IV presents the measured results. The conclusions is presented in Section V.

II. MAGNETICALLY COUPLED 2DWPT

A. The magnetically 2DWPT Fundamentals

In the proposed coil-patterned waveguide sheet, EM waves propagate while concurrently generating a magnetic field \mathbf{H} in the vicinity of the sheet. Fig.1 illustrates this process using a cross-sectional view of the waveguide sheet, specifically focusing on the behavior of EM waves following the application of a pulse wave. Within the Tx waveguide sheet, the group velocity is markedly slow. Consequently, at $t=0$, the magnetic field is confined near the area of pulse input. By $t=N$, the magnetic field has propagated directly beneath the Rx coil. The magnetic influence of the Tx waveguide sheet is localized around the Rx coil vicinity at this point.

To maintain sufficient coupling, it is necessary to minimize the air gap, which makes the proposed system less suited for powering handheld devices such as smartphones. However, since most of the EM energy is confined within the sheet, the system exhibits superior performance in terms of the SAR and electromagnetic interference (EMI).

The supplied power (P_{sup}) propagates through the sheet, reaching the Rx coil as P_{in} , which then divides into three distinct components: P_{out} , $P_{through}$, P_{return} . These components represent the power extracted by the Rx coil, the power continuing to the end of the sheet, and the power reflected back at the Rx coil, respectively.

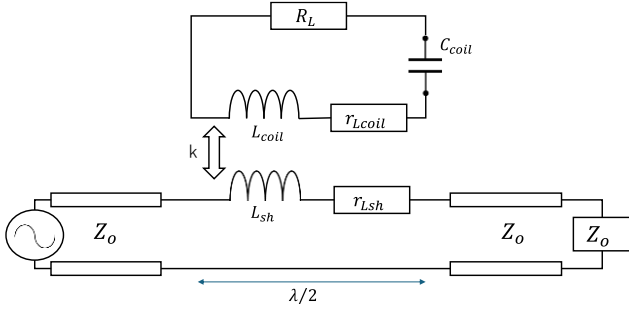


Fig. 2. Equivalent model of the magnetically coupled 2DWPT system.

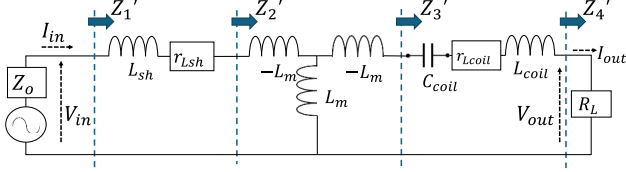


Fig. 3. Simplified equivalent circuit of Fig. 2. This circuit defines various impedances observed from different points in the circuit: Z'_1 as the impedance seen from the power source to the load, Z'_2 as the impedance just before the T-network, Z'_3 as the impedance after the T-network, and Z'_4 as the impedance from the Rx coil to the load. The voltage applied from the power source to the Z'_1 region is denoted as V_{in} , and the current as I_{in} , while the voltage and current applied to the load are V_{out} , and I_{out} , respectively.

B. Equivalent Circuit

Fig. 2 illustrates the equivalent model of the magnetically coupled 2DWPT system. In this model, the path from the power supply to the Rx coil is conceptualized as a transmission line characterized by an impedance Z_o . The section involving magnetic coupling with the Rx coil is modeled using a lumped parameter approach. At the terminus of the waveguide sheet, an absorbing boundary condition is presumed. The inductance of the sheet (L_{sh}), representing the inductance for half of the wavelength ($\lambda/2$), functions as a single transmitting coil. This coil interacts with the receiving coil through a defined coupling coefficient k . The load R_L and the resonant capacitor C_{coil} are connected in series to the Rx coil. r_{sh} , L_{coil} , and r_{coil} refer to the sheet resistance, the power receiving coil inductance.

Fig. 3 shows a simplified equivalent circuit of the model. In this circuit, the waveguide sheet extending from the power supply to the receiving coil is represented as a transmission line with impedance Z_o , and the termination is modeled as a pure resistive load, also with impedance Z_o . The sheet inductance L_{sh} and the Rx coil inductance L_{coil} , which are magnetically coupled with a coupling coefficient k , are integrated into a T-shaped circuit. This circuit includes mutual inductance L_m , as defined by (1).

$$L_m = k\sqrt{L_{sh}L_{coil}} \quad (1)$$

Fig.3 has a nonresonant-series [N-S] topology, which is a well-known circuit scheme in magnetic field coupling systems [12]. Here, the power input from the source to the Z'_1 region is denoted as P_{in} , and the power consumed by the load R_L as P_{out} . The extracted efficiency, η_{ext} , is then expressed by the following equation:

$$\eta_{ext} = \frac{V_{out}I_{out}}{V_{in}I_{in}} = \frac{R_L I_{out}^2}{Z'_1 I_{in}^2} = \frac{P_{out}}{P_{in}}. \quad (2)$$

The impedance viewed from each point to the load side is expressed by the following equation.

$$Z'_1 = Z'_2 + r_{Lsh} + Z_o + j\omega L_{sh} \quad (3)$$

$$Z'_2 = \frac{(\omega L_m)^2}{Z'_3} \quad (4)$$

$$Z'_3 = Z'_4 + r_{Lcoil} + j\left(\omega L_{coil} - \frac{1}{\omega C_{coil}}\right) \quad (5)$$

$$Z'_4 = R_L \quad (6)$$

The inductance L_{coil} of the Rx coil and the resonant capacitor C_{coil} satisfy the resonance condition shown in the following equation. ω denotes angular frequency.

$$\omega L_{coil} = \frac{1}{\omega C_{coil}} \quad (7)$$

From (2), (3), and (7), the ratio of I_{in} to I_{out} can be obtained to derive the power feed efficiency η_{ext} , which is expressed as follows:

$$\eta_{ext} = \frac{R_L(\omega L_m)^2}{r_{Lsh}(R_L + r_{Lcoil})^2 + r_{Lcoil}(\omega L_m)^2 + R_L(\omega L_m)^2 + Z_o(R_L + r_{Lcoil})^2} \quad (8)$$

Even in an ideal lossless transmission system (where $r_{Lsh} = r_{Lcoil} = 0$), the power continuing to the end of the sheet, denoted as $Z_o(R_L + r_{Lcoil})^2$, ensures that the power transfer efficiency, η_{ext} , remains below one. In addition, since $Z'_1 \neq Z_o$, the following losses Γ_l due to reflection coefficients occur.

$$\Gamma_l = \left| \frac{Z'_1 - Z_o}{Z'_1 + Z_o} \right| \quad (9)$$

When reflections are taken into account, (8) can be updated as follows:

$$\eta_A = \left| \frac{Z'_1 - Z_o}{Z'_1 + Z_o} \right| \cdot \frac{R_L(\omega L_m)^2}{r_{Lsh}(R_L + r_{Lcoil})^2 + r_{Lcoil}(\omega L_m)^2 + R_L(\omega L_m)^2 + Z_o(R_L + r_{Lcoil})^2} \quad (10)$$

where η_A denotes extracted efficiency considering return loss. The coupling coefficient improves as the wavelength λ shortens. On the other hand, the attenuation constant α , defined below, also increases.

$$\alpha = \frac{R_o}{2\lambda f L_o} \quad (10)$$

where f , R_o , L_o denotes the frequency of EM wave, resistance and inductance per unit distance of the waveguide.

In the magnetically coupled 2DWPT, there is a trade-off between extracted efficiency and propagation loss, centered on the wavelength. This relationship was carefully considered during the system design. The specific performance metrics of the system will be explored through simulations in the subsequent chapter.

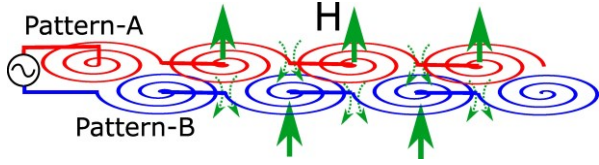


Fig. 4. Conceptual diagram of the coil-patterned sheet. The coil elements are arranged in a specific pattern and connected in series. Both pattern are arranged half a coil away from each other.

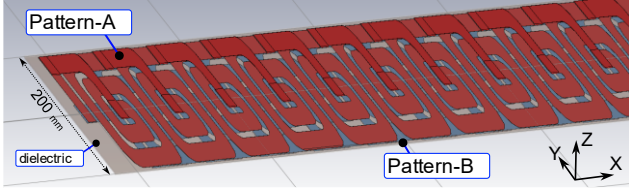


Fig. 5. Simulation model of waveguide sheet. The dielectric is assumed to be PTFE, characterized by a thickness of 0.5 mm, a relative permittivity of 2.1, and a loss tangent ($\tan\delta$) of 0.0002. The simulation software used was CST Studio Suite 2021. All boundary conditions were set to open boundary with sufficient distance from the model.

III. FULL-WAVE SIMULATION

In this chapter, we introduce the coil-patterned waveguide sheet and assess its performance through simulation. The results demonstrate that lengthening the waveguide does not significantly impact the extracted efficiency. Additionally, it is shown that the waveguide sheet can achieve adequate levels of the SAR.

A. Coil-Patterned Waveguide Sheet

A conceptual diagram of the waveguide sheet composed of coil pattern-A and B is shown in Fig. 4. Each coil pattern generates a magnetic field in the same direction, as the winding direction of the coils and the direction of the current flow are opposite. Both pattern interact to partially cancel each other's magnetic fields. As a result, a uniform magnetic field is established around the waveguide.

The simulation model of the coil-patterned sheet is shown in Fig. 5. And the physical properties obtained from the simulation are shown in Table 1. The simulation model consists of a dielectric sandwich structure incorporating two coil patterns. Common plastic is adequate for the dielectric material.

TABLE I. PHYSICAL PROPERTIES OF COIL-PATTERNED SHEET

Description	Value
Thickness [mm]	2.08
Frequency [MHz]	6.78
Characteristic Impedance [Ω]	50
Wavelength [mm]	596
Propagation Loss [dB/m]	-0.701
Group Velocity [m/s]	3,326,643.5 (90th of the speed of light)
SAR [W/kg] (at 0.5W power supply)	0.00035 (Max 5.7 kW is permissible within the sheet)

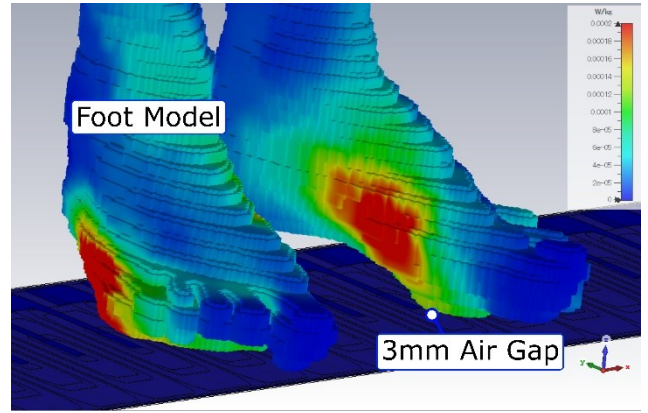


Fig. 6. The results of SAR simulation. The foot model is positioned with an air gap of 3 mm. The simulation assesses the leakage of EM waves from the sheet and their subsequent absorption.

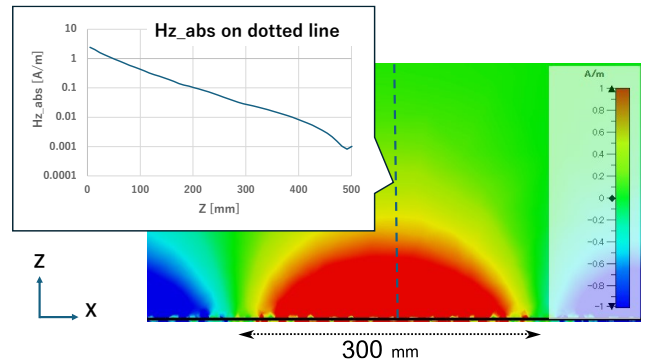


Fig. 7. Distribution of absolute value of magnetic field in Z direction in XZ plane. And the graph shows the absolute value of the magnetic field on the dot line in the figure

The inductance of the coil pattern and the capacitance within the dielectric considerably reduce the wavelength: while the vacuum wavelength at 6.78 MHz is 44.2 meters, the wavelength within the sheet is approximately 0.6 meters. Additionally, the group velocity within the sheet is decreased to 1/90th of the speed of light, causing electromagnetic energy to propagate slowly. This reduction in propagation speed ensures that extracted efficiency is preserved, even when the length of the sheet is extended.

The propagation loss simulated is -0.7 dB/m. Propagation loss can be reduced to less than 30% if the sheet length does not exceed 2 meters. Additionally, propagation loss increases as the wavelength decreases. Therefore, the wavelength should be adjusted based on the intended application to optimize performance.

SAR simulation results are presented in Fig. 6, using a human foot as the model. An air gap of 3 mm between the foot and the sheet was established to simulate the absorption of electromagnetic waves. In practical applications, a carpet or other protective layer is typically placed over the sheet, allowing for a larger air gap which is expected to further improve SAR values. Based on the simulation results and the safety standard for SAR, which is 4 W/kg, a maximum power output of 5.7 kW is permissible within the sheet.

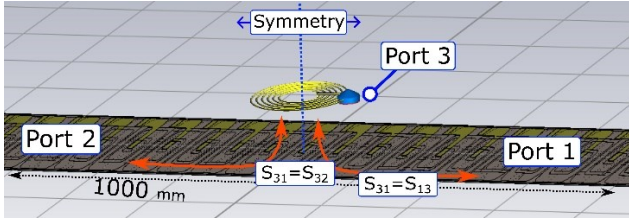


Fig. 8. Simulation model featuring the Rx coil. A 120 mm diameter Rx coil, which is made of pure copper, is centrally installed on a 1 m sheet. The air gap is set to 60 mm. The model is symmetrical, with the power receiving coil positioned at the center (indicated by a dotted line). All boundary conditions are set to open, ensuring a sufficient distance from the model to prevent interference.

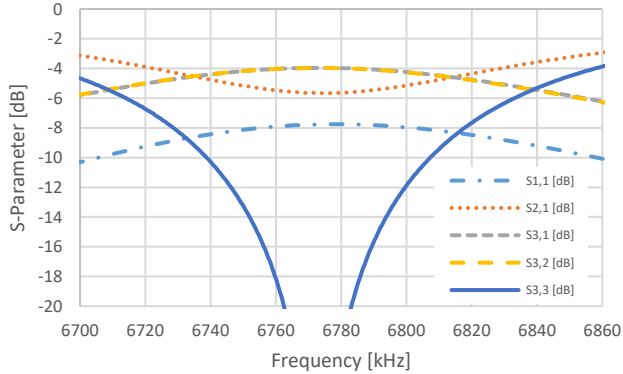


Fig. 9. The receiving coil exhibits resonance at 6.78 MHz. Due to symmetry, S31 and S32 coincide, both registering at -4 dB at 6.78 MHz.

Fig. 7 shows the magnetic field in the Z direction formed just above the waveguide sheet. Smooth wave patterns are observed in the direction of EM wave propagation (X direction). The absolute value of the magnetic field exhibits exponential decay vertically above the sheet. Consequently, the waveguide sheet does not generate a radiation field around it, effectively minimizing electromagnetic exposure.

B. Extracted Efficiency

The simulation model incorporates an additional Rx coil to verify that the length of the waveguide sheet does not influence the leakage flux. In Fig.8, The coil configuration includes a spiral coil with a 120 mm diameter, six turns, and a 60 mm air gap. Notably, in practical applications, the sheet is typically covered with a protective layer, such as a carpet, and the air gap is adjusted to accommodate the thickness of this covering.

Ports are installed at both ends of the sheet as well as on the Rx coil. The Rx coil is tuned to resonate at 6.78 MHz by connecting a capacitor in series. The model is designed symmetrically around the power receiving coil, ensuring that the S-parameters simulated from the ports at both ends of the sheet to the power receiving coil are identical (S31 equals S32). Additionally, in accordance with the reciprocity theorem, S31 and S13 are equivalent. As a result, the maximum extraction efficiency achieved is -3 dB.

The parameters of the Rx coil and the S-parameters at 6.78 MHz are given in Table 2, 3.

TABLE II. THE PARAMETERS OF RX-COIL

Description	Value	Description	Value
Inductance [uH]	2.9	Air Gap [mm]	30
Outside Diameter [mm]	120	Inside Diameter [mm]	40
Number of the Coil Turns	6	Thickness of a Wire [mm]	0.8

TABLE III. S-PARAMETER SIMULATED AT 6.78 MHz

Description	Value	Description	Value
S11 [dB]	-7.75	S31 [dB]	-3.98
S21 [dB]	-5.63	S32 [dB]	-3.99
S13 [dB]	-3.98	S33 [dB]	-22.04

Fig. 9 shows the S-parameters across different frequencies. As seen from (3) to (6), Z_1' increases as the resonance frequency is approached, leading to an increase in reflected power as indicated in (9). This is accompanied by a rise in S11, indicating increased reflection. Conversely, near the resonant frequency, the extraction of power from the coil intensifies, resulting in a decrease S21, which is the power transmitted to the opposite end of the sheet.

Given that the theoretical upper limit is -3 dB due to symmetry, and considering the increase in return loss near the resonant frequency, an S31 of -3.96 dB represents a favorable outcome.

Finally, to assess the influence of sheet length on S31, we varied the sheet length at intervals of 160 mm, which is larger than the diameter of the Rx coil. Typically, in magnetic field coupling, larger transmission coils result in increased flux leakage and a significant drop in efficiency. To mitigate the impact of propagation loss, the waveguide sheet material in the simulation was replaced with a perfect electric conductor (PEC). The simulation results are displayed in Fig. 10.

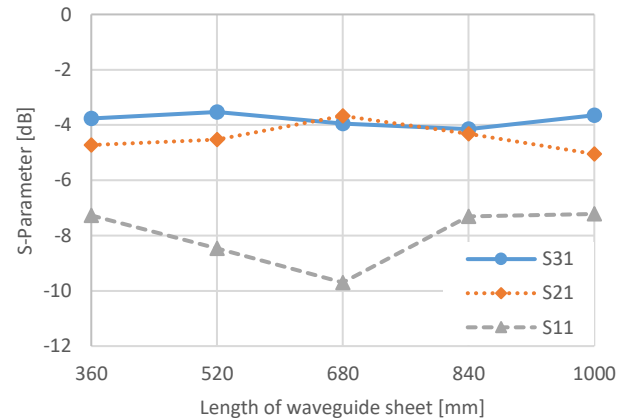


Fig. 10. S-parameters as a function of waveguide sheet length. In the simulation model depicted in Fig. 8, the coil pattern material was substituted with a perfect electric conductor (PEC). Simulations were conducted for various lengths of the waveguide sheet to analyze the effects.

The results reveal no dramatic variation in S31 with changes in sheet length, suggesting that the proposed magnetically coupled 2DWPT system can effectively and economically extend the power feeding range by increasing the sheet length.

Thus far, we have utilized simulations to assess the physical properties of the magnetically coupled 2DWPT system. In the forthcoming section, we will construct a prototype coil-patterned sheet based on the simulation model and evaluate its actual performance through experimental measurements.

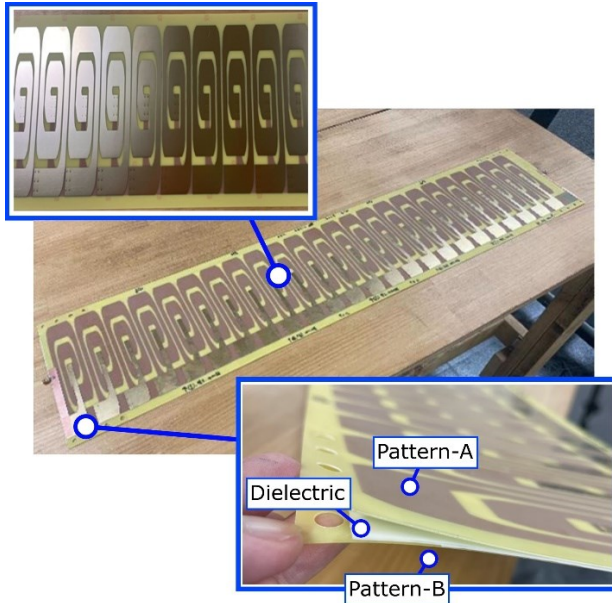


Fig. 11. Prototype coil pattern waveguide sheet. A PTFE sheet is sandwiched between FR-4 substrates with a pattern of coil elements connected in series. An SMA connector is connected to the edge of the sheet.

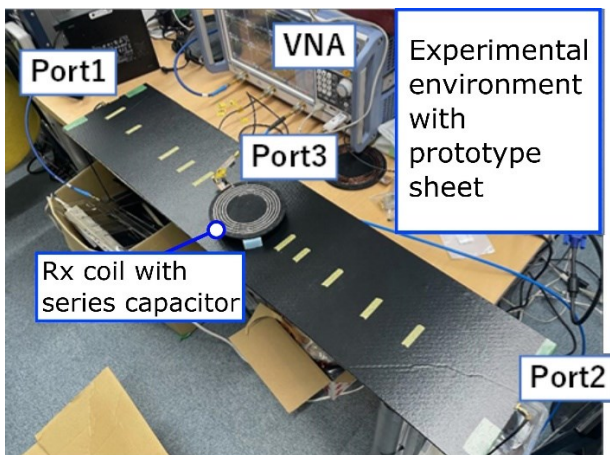


Fig. 12. Setup of power feeding performance measurement test. The Rx coil is connected in series with a capacitance to resonate at 6.78 MHz. Each port is matched with 50 Ω . S-parameters are measured at each port using a vector network analyzer (Rohde & Schwarz ZNB-20). the surface of the sheet is covered with a protective insulation cover.

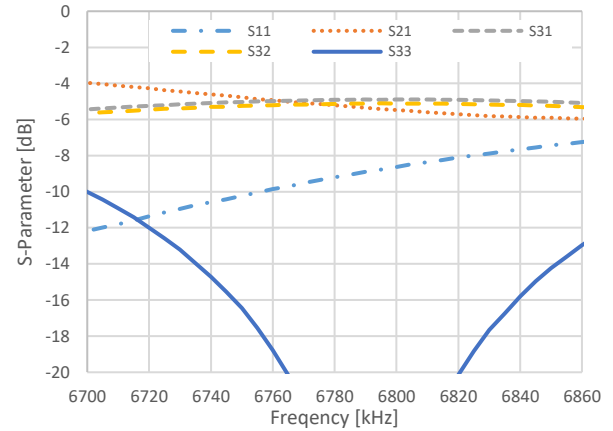


Fig. 13. Measured S-parameters. The values of S31 and S32 are almost identical because they are symmetrical around the Rx coil as in the simulation model.

IV. EXPERIMENTAL SYSTEM

A. Prototyped Coil-Patterned Sheet

The prototype coil-patterned waveguide sheet is shown in Fig. 11. The physical properties of the sheet obtained from the measurements are shown in Table IV. This prototyped sheet was fabricated using the same parameters as the simulation model shown in Fig. 5.

Input and output ports, equipped with SMA connectors, are located at both ends of the sheet. Measurements conducted with a vector network analyzer (VNA), Rohde & Schwarz ZNB-20, indicate a propagation loss of -0.968 dB, which is closely aligned with the simulation result of -0.701 dB.

TABLE IV. PROPERTIES OF PROTOTYPED COIL-PATTERNED SHEET

Description	Value
Thickness [mm]	1.8
Frequency [MHz]	6.78
Characteristic Impedance [Ω]	50
Propagation Loss [dB/m]	-0.968

B. Measurement of Efficiency

The measurement setup for evaluating extracted efficiency includes a waveguide sheet coupled with an Rx coil (Fig. 12). The Rx coil is strategically positioned at the center of the sheet and is connected in series with a resonant capacitor. The properties of the Rx coil were referenced from Table II, consistent with the simulations.

Consistent with the simulation model depicted in Fig. 8, ports are established at both ends of the sheet and on the Rx coil. Each port was connected to a VNA, and the measured S-parameters are shown in Fig. 13. Additionally, the S-parameters at 6.78 MHz are detailed in Table V.

TABLE V. S-PARAMETER MEASURED AT 6.78 MHZ

Description	Value	Description	Value
S11 [dB]	-9.19	S31 [dB]	-4.91
S21 [dB]	-5.21	S32 [dB]	-5.14
S13 [dB]	-4.91	S33 [dB]	-26.29

Compared to the simulation results, S31 decreased by approximately 1 dB in the actual measurements. This deviation may be attributed to propagation losses in the prototype sheet and additional losses that were not considered in the simulation. In the simulation, both the resonance capacitor and the matching circuit at Port 3, designed for 50 Ω impedance matching, were assumed to be lossless. However, in reality, these components do incur losses, which contribute to the observed reduction in S31.

Comparing the simulation results (shown in Fig. 8 and 9, and Table II) with the experimental findings (shown in Fig. 12 and 13, and Table IV), the measured outcomes generally align with expectations. This consistency supports the efficacy of the proposed magnetically coupled 2DWPT system, demonstrating that it can achieve robust coupling and high extracted efficiency, even with a waveguide sheet that extends significantly beyond the dimensions of the Rx coil.

V. CONCLUSION

In this paper, we introduced a magnetically coupled 2-Dimensional Waveguide Power Transfer (2DWPT) system, featuring a coil-patterned waveguide sheet designed to overcome common challenges in wireless power transfer, such as efficiency loss due to leakage flux and limited transfer distance. The full-wave simulations and subsequent experimental validations have demonstrated that the proposed system maintains high efficiency and consistent power delivery across extended lengths of the waveguide sheet.

The results from the simulations showed that the proposed coil-patterned waveguide sheet effectively minimized the leakage flux while maintaining a uniform magnetic field across the sheet. The waveguide sheet can be extended without a significant drop in efficiency. The simulation results show that the extracted efficiency does not drop significantly with the length of the waveguide sheet. Due to the symmetric simulation model, the maximum extracted efficiency is -3 dB (50 %). The simulated suction efficiency is -3.98 dB, which is within -1 dB of the theoretical limit.

The prototyped waveguide sheet demonstrated that a propagation loss close to simulated values. The measured S-parameter results were generally close to the simulation results, although the extracted efficiency (S31) was about -1 dB lower than the simulation results. The decrease in S31 was within a reasonable range because the experimental system includes losses that were not considered in the simulation model.

In practice, the ability to extend the waveguide sheet without diminishing efficiency offers significant advantages for real-world applications like a dynamic WPT. The proposed system can safely extend the range of WPT by extending the waveguide sheet. The waveguide sheet is made of copper and plastic and is inexpensive. Future work will focus on optimizing the design of coil pattern and frequency.

ACKNOWLEDGMENT

This work was supported by JSPS KAKENHI Grant Number 21K14155.

REFERENCES

- [1] H. Kim et al., "Coil design and measurements of automotive magnetic resonant wireless charging system for high-efficiency and low magnetic field leakage," in *IEEE Transactions on Microwave Theory and Techniques*, vol. 64, no. 2, pp. 383-400, Feb. 2016.
- [2] Q. Zhu, M. Su, Y. Sun, W. Tang and A. P. Hu, "Field orientation based on current amplitude and phase angle control for wireless power transfer," in *IEEE Transactions on Industrial Electronics*, vol. 65, no. 6, pp. 4758-4770, June 2018.
- [3] R. Bosshard, U. Iruretagoyena and J. W. Kolar, "Comprehensive evaluation of rectangular and double-D coil geometry for 50 kW/85 kHz IPT system," in *IEEE Journal of Emerging and Selected Topics in Power Electronics*, vol. 4, no. 4, pp. 1406-1415, Dec. 2016.
- [4] Y. Li, J. Zhao, Q. Yang, L. Liu, J. Ma and X. Zhang, "A novel coil with high misalignment tolerance for wireless power transfer," in *IEEE Transactions on Magnetics*, vol. 55, no. 6, pp. 1-4, June 2019.
- [5] A. Mahesh, B. Chokkalingam and L. Mihet-Popa, "Inductive wireless power transfer charging for electric vehicles—a review," in *IEEE Access*, vol. 9, pp. 137667-137713, 2021.
- [6] T. Fujita, T. Yasuda and H. Akagi, "A dynamic wireless power transfer system applicable to a stationary system," in *IEEE Transactions on Industry Applications*, vol. 53, no. 4, pp. 3748-3757, July-Aug. 2017.
- [7] S. Laporte, G. Coquery, V. Deniau, A. De Bernardinis, and N. Hautiere, "Dynamic wireless power transfer charging infrastructure for future EVs: From experimental track to real circulated roads demonstrations," *World Electric Vehicle Journal*, vol. 10, no. 4, pp. 84, 2019.
- [8] J. Rahulkumar. et al., "An empirical survey on wireless inductive power pad and resonant magnetic field coupling for in-motion EV charging system," *IEEE Access*, vol. 11, pp. 4660-4693, 2023.
- [9] H. Shinoda, Y. Makino, N. Yamahira and H. Itai, "Surface sensor network using inductive signal transmission layer," 2007 Fourth International Conference on Networked Sensing Systems, Braunschweig, Germany, 2007, pp. 201-206.
- [10] A. Noda and H. Shinoda, "Selective wireless power transmission through high-Q flat waveguide-ring resonator on 2-D waveguide sheet," in *IEEE Transactions on Microwave Theory and Techniques*, vol. 59, no. 8, pp. 2158-2167, Aug. 2011.
- [11] The International Commission on Non-Ionizing Radiation Protection, "Guidelines for limiting exposure to time-varying electric, magnetic, and electromagnetic fields (up to 300 GHz)," *Health Phys.*, vol. 74, no. 4, pp. 494-522, Apr. 1998.
- [12] T. Imura and Y. Hori, "Unified theory of electromagnetic induction and magnetic resonant coupling," in *IEEJ Transactions on industry applications*, vol. 199, no. 2, pp. 58-80, April 2017.